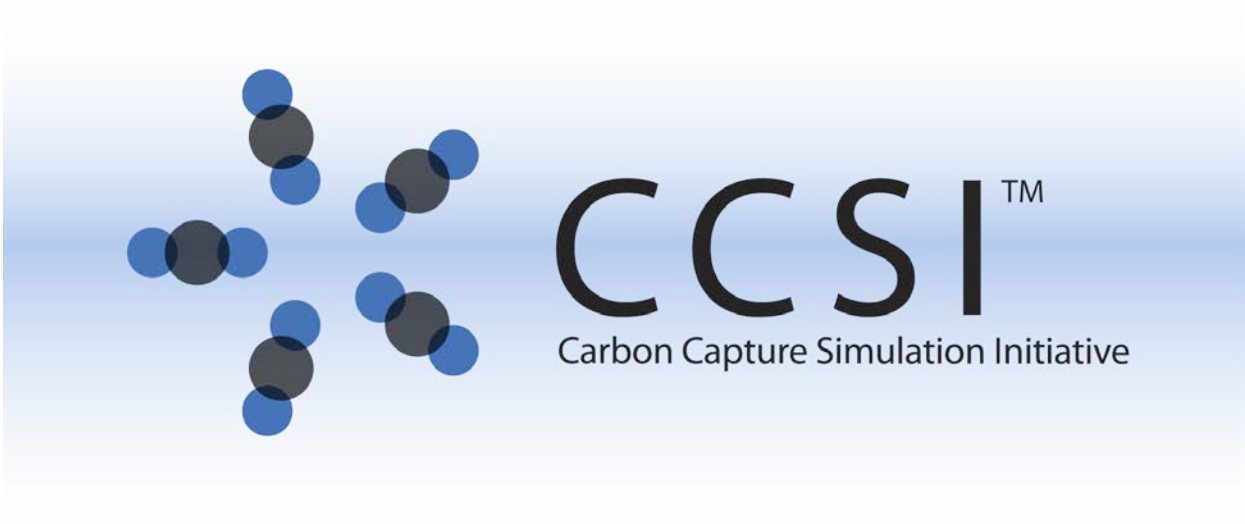

Report on liquid film flow over an inclined plate: effect of solvent properties

Work Performed Under
Carbon Capture Simulation Initiative

Prepared by
National Energy Technology Laboratory, Albany, Oregon 97321
In collaboration with
Pacific Northwest National Laboratory and Princeton University

12 September 2014

Disclaimer

This report was prepared as an account of work sponsored by an agency of the United States Government. Neither the United States Government nor any agency thereof, nor any of their employees, makes any warranty, express or implied, or assumes any legal liability or responsibility for the accuracy, completeness, or usefulness of any information, apparatus, product, or process disclosed, or represents that its use would not infringe privately owned rights. Reference herein to any specific commercial product, process, or service by trade name, trademark, manufacturer, or otherwise does not necessarily constitute or imply its endorsement, recommendation, or favoring by the United States Government or any agency thereof. The views and opinions of authors expressed herein do not necessarily state or reflect those of the United States Government or any agency thereof.

Reference herein to any specific commercial product, process, or service by trade name, trademark, manufacturer, or otherwise, does not necessarily constitute or imply its endorsement, recommendation, or favor by the United States Government, the Department of Energy, or the National Energy Technology Laboratory. The views and opinions of authors expressed herein do not necessarily state or reflect those of the United States Government, the Department of Energy, or the National Energy Technology Laboratory, and shall not be used for advertising or product endorsement purposes.

Table of Contents

1. Abstract 1
2. Background & Introduction 1
3. Method 3
4. Computational Setup & Numerical Formulation 4
5. Solvent Properties 6
6. Results & Discussion 7
   6.1 Comparison with Experiments 8
   6.2 Effect of the Solvent Properties and Inclination Angle 9
      6.2.1 Film Thickness 9
      6.2.2 Interfacial and Wetted Area 12
   6.3 Effect of Contact Angle 16
7. Final Summary 20
References 22

List of Figures

Figure 1: Schematic of a structure packing tower showing the countercurrent gas-liquid flow. Exploded view shows the orientation of the corrugated packing sheet inside the tower (*Koch-Glitsch: http://www.koch-glitsch.com/default.aspx)*. 2
Figure 2: Schematic of the computational flow domain. Liquid flows down from top of the inclined smooth plate. 5
Figure 3: Discretization of the computational flow domain showing the grid. Near the plate, a very fine mesh is used in order to capture the flow field. The center of the domain is also meshed very finely to capture the rivulet flow dynamic 6
Figure 4: Effect of the inertia on the flow pattern over the inclined plate. Flow develops from droplet to rivulet and finally to full film (a fully wetted plate). 9
Figure 5: Comparison of the computed normalized wetted area of the plate with experimental results of Hoffman et al (2005) at different Weber numbers. In the validation, water is used as solvent. 9
Figure 6: (a) Development of film profile over an incline plate at a fixed flow rate, red solid line: Ka=4164 and green double dotted line: Ka=15. The lower value of the Kapitza number corresponds to highly viscous solvent. (b) Comparison of the computed film thickness with Nusselt theory [26] at different Kapitza numbers. (c) Scaling of the film thickness with Ka shows the relation as $\delta \sim 1\mathrm{Ka}1/4$. 11
Figure 7: (a) Variation of the computed film thickness with Kapitza number at two Weber number. Note that at both We values, the plate is fully wetted. (b) Scaling of the film thickness with Ka shows relation as $\delta \sim 1\mathrm{Ka}1/4$. (c) Scaling of film thickness and flow rate with Ka. 12
Figure 8: (a) Schematic of the flow domain used for the study of rivulet flow. (b) Transient evaluation of the wetted area of the plate for different solvents. (c) Variation of the interfacial and wetted area of plate with Kapitza number at fixed flow rate 2×10^{-6} m^3/sec. Inset shows shape of interface (*f* = 0.50) for different solvents. 13
Figure 9: (a) Variation of the normalized interfacial area with Kapitza number for different inlet widths at fixed flow rate 2×10^{-6} m^3/sec. (b) Scaling for the variation of the interface area with Ka shows that $AIn \sim 1/\mathrm{Ka}1/2$. (c) Shape of the interface (*f*=0.50) for different inlet width at Ka=15. The developed width of the rivulet is insensitive to inlet size at a fixed flow rate. 14
Figure 10: Variation of the normalized interfacial area with Kapitza number for different flow rate at inclination angle 60° and fixed inlet size (2x20mm). 15
Figure 11: Variation of A_{In} with Ka for different inclination angles at a flow rate 2×10^{-6} m^3/sec and fixed inlet size (2x20mm). Inset show the percentage change in the interfacial area with respect to the interfacial area corresponding to θ=60°. 16
Figure 12: Variation of the computed film thickness with Kapitza numbers at two contact angles for the fully wetted plate at fixed flow rate of $1.05\text{x}10^{-5}$ m^3/s 17
Figure 13: (a) Variation of the Interfacial and wetted areas with contact angle. (b) Variation in interfacial area normalized with respect to the interfacial area corresponding to γ = 70°. (c) Scaling of the interfacial and wetted areas with $(1-\cos\gamma)^{-m}$ for 2 solvents having Ka=15 (low σ) and Ka=783 (high σ). 18
Figure 14: Scaling (a) wetted area and (b) interfacial area with contact angle and Kapitza number. For an inclined plate having θ = 60° at a fixed flow rate and inlet area (2x20mm). 20

List of Tables

Table 1: Solvents used in the simulation 7

1. Abstract

Film flow down an inclined plate is numerically investigated using the Volume of Fluid (VOF) multiphase method. Flow simulations have been systematically carried out for a wide range of parameters such as varying inlet cross-section, flow rate, plate inclination angle, range of solvent properties and contact angles. Based on results of rigorous and extensive simulations, scaling theory is being proposed for interfacial and wetted areas and film thickness.

A theory is proposed based on numerical simulation for film thickness and interfacial and wetted areas in terms of Kapitza number (Ka). The major advantage of the Kapitza number is that it depends only on fluid properties: surface tension, viscosity, and density and independent of flow variable. Accordingly, it is fixed for each fluid and it decreases with increased solvent viscosity. For fully wetted plate, achieved with an inlet cross-section spanning the width of the domain, the film thickness varies as $1/\mathrm{Ka}^{1/4}$. To investigate the effects of solvent viscosity on wetted area and interfacial area the simulation setup was modified to use a smaller inlet cross-section. In this case, as expected, interfacial and wetted area deceases with increased value of Ka. A scaling for interfacial and wetted areas and Kapitza number are proposed:

This information may be used in the design of structure packing elements, such as one would find in solvent absorption. Included in a separate document available on SVN is a case study for film flow down an inclined plate and instructions on the simulation setup.

2. Background & Introduction

Solvent absorption is usually carried out in a countercurrent gas liquid flow in the tower, where the gas flows upward and liquid falls in downward direction. The purpose is to preferentially dissolve one or more of the constituents of the gas, such as carbon dioxide (CO_2), into the liquid. The tower is filled with a packing material that provides enhanced surface area for gas-liquid contact. Surface area is important because very little reaction will occur without adequate contact of the gas and liquid. Structured packing is popular because it provides a large surface area for mass transport between both phases while minimizing pressure drop. This packing is generally made of corrugated sheets arranged in crisscrossing fashion to form a single layer of packing material (see Figure1). Accurate design of the packed column requires knowing essential hydraulic characteristics of the packing element across the operating range. Computational fluid dynamics (CFD) model is a useful tool to capture local hydrodynamics and complex behaviors associated with chemical reaction, mass transfer, etc.

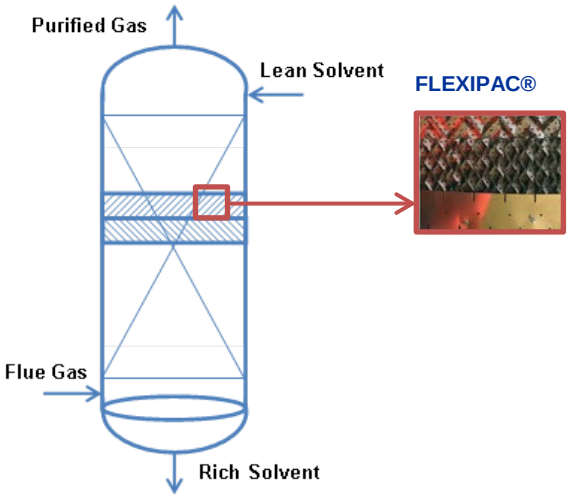

Figure 1: Schematic of a structure packing tower showing the countercurrent gas-liquid flow. Exploded view shows the orientation of the corrugated packing sheet inside the tower (*Koch-Glitsch: http://www.koch-glitsch.com/default.aspx)*.

Absorption columns are characterized by length scales of several meters with diameters that may range from 5- 10 m and overall column heights of 20-30 m. In contrast, the characteristic dimensions of the packing are much smaller with the length scale of a typical layer of corrugated structured packing on the order of 20 centimeters [1]. Finally, the dimension of liquid film thickness is on the order of tenths of millimeters for structured packing. The detailed behavior of wetting flow in the packing element and the macro-level flow distribution through the packing are key factors influencing the efficiency of the column. These scales cannot be resolved simultaneously within a single computational model. That is, it is computationally infeasible to run computations at large scales while taking into account the local gas-liquid interactions and the real geometry of the packing. This problem requires a multi-scale approach [2].

One of the ideas being proposed is the use of Volume of Fluid (VOF) simulations, which are suitable technique for small scale, to develop closure models needed for a device scale multiphase Eulerian-Eulerian based simulation. In the present effort, VOF simulations have been used to develop a better understanding of the behavior at the micro scale.

Gravity driven film flowing down an inclined plate provides the simplest configuration for studying the hydrodynamics of structured packing. The fluid dynamics of liquid films is important because efficiency of CO_2 absorption is closely related to structure of liquid films within the packing. Liquid films can exhibit a range of flow regimes: full film, rivulet and droplets. These features are dependent upon various flow parameters (e.g., liquid flow rate, plate surface texture, plate geometry, etc.), and liquid properties (viscosity, density, surface tension). The hydrodynamics and the reactive mass transfer characteristics of liquid films in a small element of packing material can significantly impact the behavior of the column. Full films provide greatest efficiency because of large surface area conducive to CO_2 absorption. Formation of rivulets or any other phenomena reduces the wetted area of the packing and hinders heat and mass transfer.

As noted the problem of gravity driven film flow involves a number of parameters. While a number of studies have examined the impact of such parameters on wetting phenomena [3-7] , they typically report the behavior in the context of a single physical property. The result is information for one particular property and/or a correlation that depends on each physical property independently [5, 7-11]. The effects of viscosity on wetted area and film thickness at moderate value of viscosity (~2.5 mPa-s) have been investigated using VOF simulation [4, 7, 12] and experiment [9]. However, some disagreement exists. The effect of the inclination angle on the wetted area and film thickness has also been studied analytically [13], experimentally [14] and numerically using VOF method [8, 15]. The goal of the current effort is to conduct a systematic series of simulations in order to get a collective understanding of all physical properties as a single function. Ultimately this simple setup may be used as a stepping stone to more complicated scenarios: multiphase counter-current flow, counter-current flow between two corrugated sheets, including texture (corrugation) to the plate in various orientations, including mass transfer effects, etc.

3. Method

In this effort Volume of Fluid (VOF) multiphase flow simulations are being used to investigate gravity driven film flow down an inclined plate. The VOF model is a surface tracking technique applied to a fixed Eulerian grid when knowing the interface between two or more immiscible fluids is of interest. This method was developed by Hirt and Nichols [16] for tracking the interface between two or more non-interpenetrated phases. It is well adapted for stratified flow as liquid film in packing's.

A brief sketch of the VOF method is provided here. For a more detailed explanation see the user manual of Ansys FLUENT 14.0 [17], which is the commercial software used to conduct the present simulations. In this approach the entire flow field is treated as a single phase. Therefore, the Navier Stokes equations are solved for a single shared field among phases.

$$\nabla \cdot \mathbf{u} = 0 \tag{1}$$

$$\frac{\partial(\rho \mathbf{u})}{\partial t} + \nabla \cdot (\rho \mathbf{u}\mathbf{u}) = -\nabla p + \mu \nabla \cdot \left(\nabla \mathbf{u} + \left(\nabla \mathbf{u} \right)^T \right) + \rho \mathbf{g} + \mathbf{F} \tag{2}$$

Here **u** is the velocity, ρ the density, *p* is the pressure, μ is the viscosity, **g** is gravitational acceleration, and **F** represents additional forces terms that depend on the problem. Accordingly, the terms on the right-hand side of the momentum equation represent the pressure forces, stress/shear forces, gravitational forces and additional force due to surface tension. The velocity in each cell is the mass averaged value of velocity of all phases present in that cell. Note that the momentum equation involves the volume fractions of both phases via the physical properties of the phases such as density and viscosity. Turbulence is not taken into account since the range of the Reynolds number of the liquid flow in this present study indicates laminar flows.

For problems studying wettability on a surface an additional force arises from the effect of surface tension. Surface tension is a force that acts only at the interface and is required to maintain equilibrium in such instances: it acts to balance radially inward intermolecular attractive force with the radially outward pressure gradient force across the surface. The continuum surface force (CSF) method of Brackbill [18] has been employed extensively to model surface tension for interfacial flows using VOF. In it the surface tension force, which produces a jump in the normal traction across the interface, is expressed as a singular body force.

$$\mathbf{F} = \sigma \frac{\rho \kappa \nabla f}{\frac{1}{2}\left(\rho_g + \rho_l\right)} \tag{3}$$

where σ is the interfacial tension (which in CSF is constant and homogeneous, therefore no Marangoni effects), κ is the local curvature of the interface and ∇f shows the direction vector. The surface tension force is distributed over a thin interfacial layer.

The interface between the phases is tracked by solving addition transport equation of scalar *f* (4). Note that the value of *f* varies from 0 to 1 (0 mean cells filled with gas and 1 corresponds to liquid).

$$\frac{\partial f}{\partial t} + \mathbf{u}.\nabla f = 0 \tag{4}$$

The advantage of two phase flow simulation is that the above equation (4) is solved only for secondary phase, and volume fraction of the primary phase is computed by satisfying constraint $\sum_{i=1}^{n} f_i = 1$.

In FLUENT, the VOF method includes the effects of surface tension along the interface between phases and along the intersection of the phases and wall through the specification of contact angle (γ). In Fluent the boundary condition is not imposed at the wall itself, but instead the contact angle that the fluid is assumed to make with the wall is used to adjust the surface normal in cells near the wall.

4. Computational Setup & Numerical Formulation

In this report wetting of an inclined plate for downward liquid film flow is examined. A schematic of the simulation setup is presented in Figure 2.

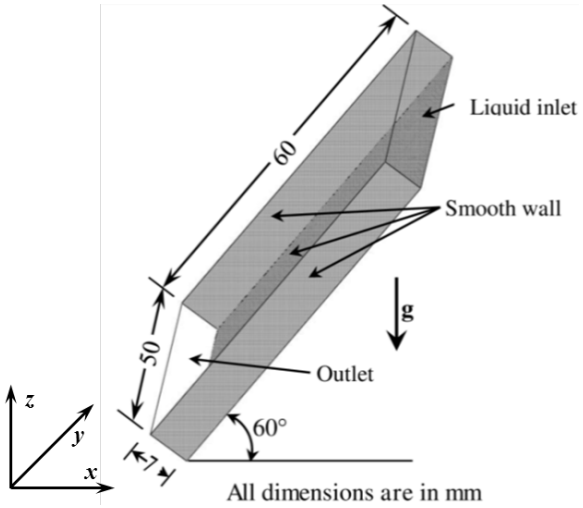

Figure 2: Schematic of the computational flow domain. Liquid flows down from top of the inclined smooth plate.

The domain consists of a stainless steel smooth plate with dimensions 60 mm long by 50 mm wide and inclined at an angle of 60° with respect to the horizontal. The depth of the domain was taken as 7 mm. Similar configurations have been used by others [4, 5, 12] and it was chosen due to the availability of experimental results that can be used for validation. These are multiphase simulations consisting of a gas and a liquid. In the present effort the gas phase is always taken as stagnant air at 25° (density ρ = 1.185 kg/m^3, viscosity $\mu = 1.831\times10^{-5}$ Pa-s) while the properties and flow of the liquid phase are varied depending on the particular simulation study. Regardless, the liquid phase enters the domain at the top and exits the bottom due to the presence of gravity.

The plate and side walls were set as no-slip walls with a static contact angle. The outlet and top boundary were set to pressure outlets with zero gauge pressure. The liquid inlet was defined as a uniform film flow given by a constant velocity perpendicular to the boundary. Unless otherwise said, the dimension of the liquid inlet was given by the width of the plate (50 mm) and the depth of the domain (7 mm). For studying rivulet flow the size of the inlet was reduced. In this case the remaining part of the inlet cross section was specified as a pressure outlet boundary with zero gauge pressure.

The computational grid is made very fine to ensure accurate resolution of the liquid flow. . Proper meshing is also a critical step in simulation in order to achieve converged and accurate results. The grid is non-uniform such that the density inside the liquid film and near the interfacial surface region is finer than the region adjacent to the surrounding gas. The number of meshes in the domain was varied with 1.26-1.50M, depending on the case. The discretization of the computational domain is shown in Figure 3.

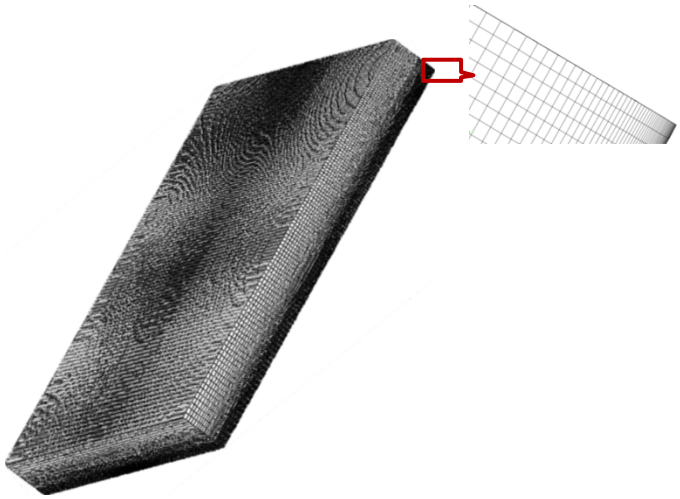

Figure 3: Discretization of the computational flow domain showing the grid. Near the plate, a very fine mesh is used in order to capture the flow field. The center of the domain is also meshed very finely to capture the rivulet flow dynamic.

The transient flow simulations were carried out using Ansys Fluent 14.0 based on cell centered finite volume approach to solve the partial differential equation using segregated solver. The geometric reconstruction scheme that utilizes the piecewise linear interface calculation (PLIC) is used to discretize the interface construction. PLIC method more accurately captures the interface than other methods, such as, Modified HRIC, CICSAM. An explicit solution scheme with conjunction of algebraic multi-grid (AMG) method has been used for faster convergence. Coupling between velocity and pressure has been established by PISO algorithm [19]. Convergence of the solution was assumed when sum of normalized residual for each conservation equation was less than or equal to 10^{-5}. The simulation is assumed to have reached pseudo-steady state when the mass flow at the exit and wetted area of the plate are constant. In addition, the stability of the transient simulation is controlled by Courant–Friedrichs–Lewy (CFL) condition and it is satisfied by value of global Courant number as 0.50. A very small time step, varying from 10^{-5}–10^{-4}, is employed in the simulation to satisfy this condition. As a result these simulations become very computationally expensive.

5. Solvent Properties

A number of organic compounds are being used for post combustion carbon capture solvents in structured packing columns. Therefore to achieve a more physically representative setup, numerical simulations were conducted using some of those compounds as the liquid phase. Specifically, aqueous solutions of Monoethanolamine (MEA) [19-21], 2-Aminomethylpropanol [22], N-Methyldiethanolamine (MDEA) [23], 1-Methyle piperazine (1MPZ) [24] at different concentrations were used to cover a wide range of solvent properties (see Table 1). Values for their physical properties, viscosity, density and surface tension, are taken from the open literature. As evident this solvent list covers a wide range of viscosities (0.9–35 mPa.s). In regard to surface tension, this list may be divided into three categories, high (~72 mN/m), medium (50mN/m) and low (~30mN/m)

tensions. The corresponding contact angle of each solvent is not available in open literature. Consequently, the contact angle is held constant at 70° in the first set of simulation studies. The impact of varying contact angle is then examined. Note that Zisman and coworkers [25]observed that the contact angle varies with solvent surface tension for a given solids substrate.

Table 1: Solvents used in the simulation

Solvent	μ_l (mPa.s)	ρ_l (Kg/m^3)	σ (mN/m)	Ka
Water	0.89	997.0	72.80	3969
20%MEA	1.18	996 [19]	57.8 [20]	2173
30% MEA	2.52	988 [19]	55.0 [20]	750
26.73% AMP by Wt [22]	2.70	995.8	43.01	534
40% MEA	3.71	979 [19]	54.80 [20]	450
0.0725*x*MPZ [24]	5.56	1005.3	54.42	258
48.8% MDEA	9.25	1016.6	47.56	117
0.10*x* MPZ[24]	10.75	1000.9	47.25	93
0.51*x* MPZ [24]	13.36	946.41	34.37	50
0.41*x* MPZ [24]	23.48	962.20	35.89	25
0.31*x* MPZ [24]	36.42	981.31	38.40	15

6. Results & Discussion

In the following section the simulation results and corresponding analysis for downward film flow over an inclined plate are presented. As noted the wetting phenomenon is controlled by many parameters such as physical properties, solvent flow rate (Q), contact angle (γ), plate inclination angle (θ), etc. Therefore it is necessary to identify the representative dimensionless groups for this problem. In this effort all results are given in terms of the Kapitza number (Ka) and the Weber number (We) or flow rate.

The Weber number (We) gives the ratio of inertia to surface tension and is one of the dimensionless groups often used to characterize this type of flow. In this effort the dimensionless group is formulated based on traditional Nusselt theory for falling film thickness

$$\mathrm{We} = \frac{\rho_l V_N \delta_N}{\sigma} \tag{5}$$

where, δ_N and V_N are thickness and velocity of the liquid film based on Nusselt theory. The pioneering work for film thickness was described in the early 20th century by Nusselt [26]. In his analysis, the effects of surface tension were absent. Surface tension is known to play an important role on the interface between fluids.

The Kapitza number (Ka) has been used in wavy vertical film flow and is an extension of classic Nusselt theory. The advantage of the Kapitza number is that it only depends on the physical properties of the fluid and is

independent of the flow parameters. Accordingly, it is fixed for each fluid with highly viscous fluids corresponding to low Ka.

$$Ka = \frac{\sigma}{\rho_l \nu_l^{4/3} g^{1/3}} \tag{6}$$

In this study the wetted area for different solvents at various Weber numbers (We) is examined. In order to maintain constant Weber number for solvents having different physical properties, the flow rate for each solvent was adjusted using the following expression:

$$Q = W\left(\frac{3\mu_l We^3}{\Delta\rho g \sin\alpha}\right)^{1/5}\left(\frac{\sigma}{\rho_l}\right)^{1/5} \tag{7}$$

6.1 Comparison with Experiments

For validation purposes, the predictions from the simulation are first compared with the results from available experiments [27] and later with predictions from Nusselt film theory [26]. Hoffmann et al [27] experimentally investigated downward film flow over a plate inclined 60° to horizontal using water (Table 1) and stagnant air at 25°C (density = 1.185 kg/m^3, viscosity = 1.831×10^{-5} Pa-s). In this effort, the wetted area was measured for different Weber numbers by varying the liquid flow rate from 1.05×10^{-6} to 1.05×10^{-5}. Thus, the impact of inertia on the resulting wetted phenomena was studied. In the experiment, the plate was found to be fully wetted for We above 0.90. Note that at higher Weber number, the inertia force dominates over the restoring surface tension force and a fully wetted film is observed. Figure 4 shows snapshots of the interface for different Weber number where a value of volume fraction *f=0.50* is used to define the liquid-gas interface [8]. At very low Weber number a droplet is observed. At low Weber numbers the surface tension dominates over the inertial force. The surface tension force tends to reduce the surface area thereby reducing the surface energy. Further increases in the flow rate correspond to rivulet flow. At higher flow rate, increased inertia gives rise to a fully wetted plate (We=1.10).

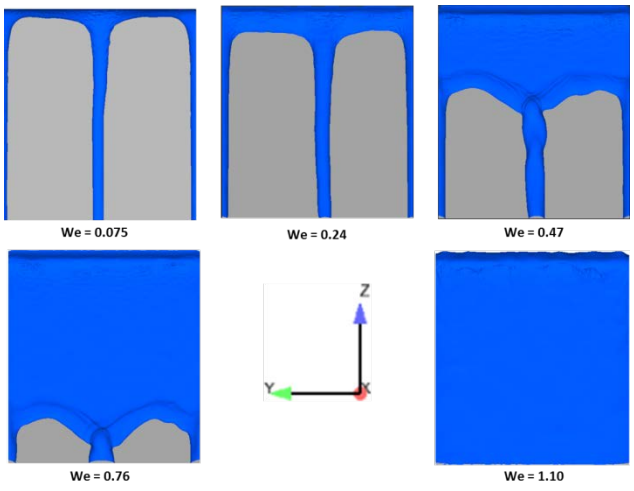

Figure 4: Effect of the inertia on the flow pattern over the inclined plate. Flow develops from droplet to rivulet and finally to full film (a fully wetted plate).

The simulation results for wetted area are compared with those from experiments in Figure 5. Here the wetted area is normalized by the actual area of the plate. As evident the simulation results compare well with experiment. Also included in the figure are the results from a separate numerical simulation by the same group, which systematically under predicts the wetted area [28]. This study demonstrates that the current simulations using the VOF method are a valid tool for conducting further studies on film flow over an inclined plate.

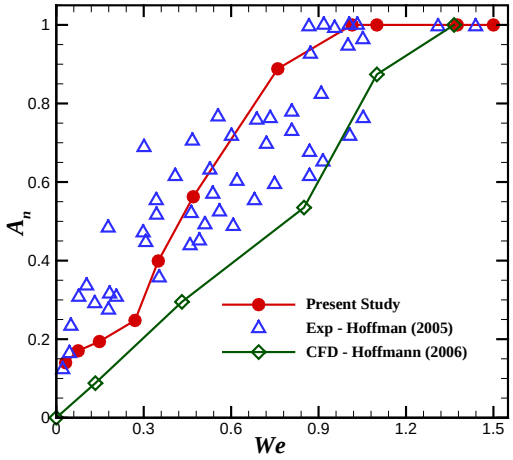

Figure 5: Comparison of the computed normalized wetted area of the plate with experimental results of Hoffman et al (2005) at different Weber numbers. In the validation, water is used as solvent.

6.2 Effect of the Solvent Properties and Inclination Angle

Apart from liquid inertia the physical properties of the liquid also play a significant role in the liquid film behavior (i.e., liquid thickness, interfacial area) and therefore on the mass transfer between liquid and gas. Film thickness may govern heat transfer between the wall and liquid while the interfacial area (free surface area) is particularly important to the mass transport between liquid and the surrounding gas. In this section, the effect of fluid properties is examined in terms of the Kapitza number to get a collective effect of all fluid parameters.

The impact of solvent properties on film thickness for a fully wetted plate using an inlet spanning the width of the domain was examined first. This setup does not reveal the variation of interfacial and wetted areas with solvent properties. Therefore, a slightly different setup was used to consider this aspect wherein the size of the inlet reduced from the entire cross section to a point inlet. The impact of inclination angle on and contact angle were also examined in both cases.

6.2.1 Film Thickness

Film thickness was examined first. During the course of this investigation it was found that some simulations required an extended length of time (> 2seconds) to ensure steady state had been achieved in regard to wetted area. At 2 seconds a non-monotonic variation of wetted area with Ka for fixed We number was observed (Figure not shown) where the wetted area would first increase and then decrease with decreasing Ka

values (i.e., increasing viscosity). However, this behavior was attributed to unsteady behavior in the simulation with regard to wetted behavior. Namely, simulations with smaller value of Ka (higher viscosity) were observed to require more time to reach a fully wetted plate than those with larger value of Ka (lower viscosity). With a further increase in total run time the simulations predicted a fully wetted plate for all Ka examined. This finding offers one possible explanation to a contradiction noted in the literature on the effects of solvent viscosity on wetted area for certain We number. Namely, Shi and Mersmann [29] first observed an increase in wetted with an increase in solvent viscosity and then a decrease with further increases in solvent viscosity (similar to the present study). In contrast, Sebastia-Saez et al. [12] only observed an increase in wetted area with increase in solvent viscosity. Finally Nicolaiewsky et al [9] observed a decrease in wetted area with solvent viscosity. Sebastia-Saez et al. was restricted to small values of solvent viscosity, while Shi and Mersmann and Nicolaiewsky used a very wide range of solvent viscosity.

In this study the flow rate is chosen in such a way that the plate becomes fully wetted for all solvents examined. An average film thickness (δ) was calculated at a sufficient distance away from the inlet and outlet to avoid entrance and exit effects. Figure 6(a) shows the volume fraction profile in the *xz*-plane s at the central line for two different solvents at a fixed flow rate of 1.05×10^{-5} m^3/sec. As evident the liquid film quickly gains uniform thickness and film thickness is greater with decreased Ka value. This observation is more clearly seen in a plot of film thickness as a function of Ka (Figure 6(b)). Also displayed is the film thickness predicted from Nusselt theory with $\delta_N = \left(3\mu_l.Q_l/\Delta\rho g \sin\alpha w\right)^{1/3}$ at a fixed flow rate. An excellent match between the VOF simulations and Nusselt theory [26] is obtained with only small discrepancy apparent. The difference is due to capillary effects at the side walls; recall the simulation reports an average film thickness across the plate. A plot for film thickness and Ka shows strong scaling, as $\delta \sim 1/\mathrm{Ka}^{1/4}$ for a fixed flow rate (Figure 6(c)).

Note that unlike the VOF simulation conducted here, Nusselt theory does not account for the effects of surface tension in the computation of film thickness. Excellent agreement between the two methods in the present effort indicates that surface tension does not play a role on the mean film thickness in the wavy laminar region. Regardless of its impact on film thickness, surface tension is an important property of the fluid that dictates the shape of liquid-gas interface, and therefore the heat and mass transfer properties of a solvent absorption column. In view of this, surface tension at the interface has been included in the present simulations.

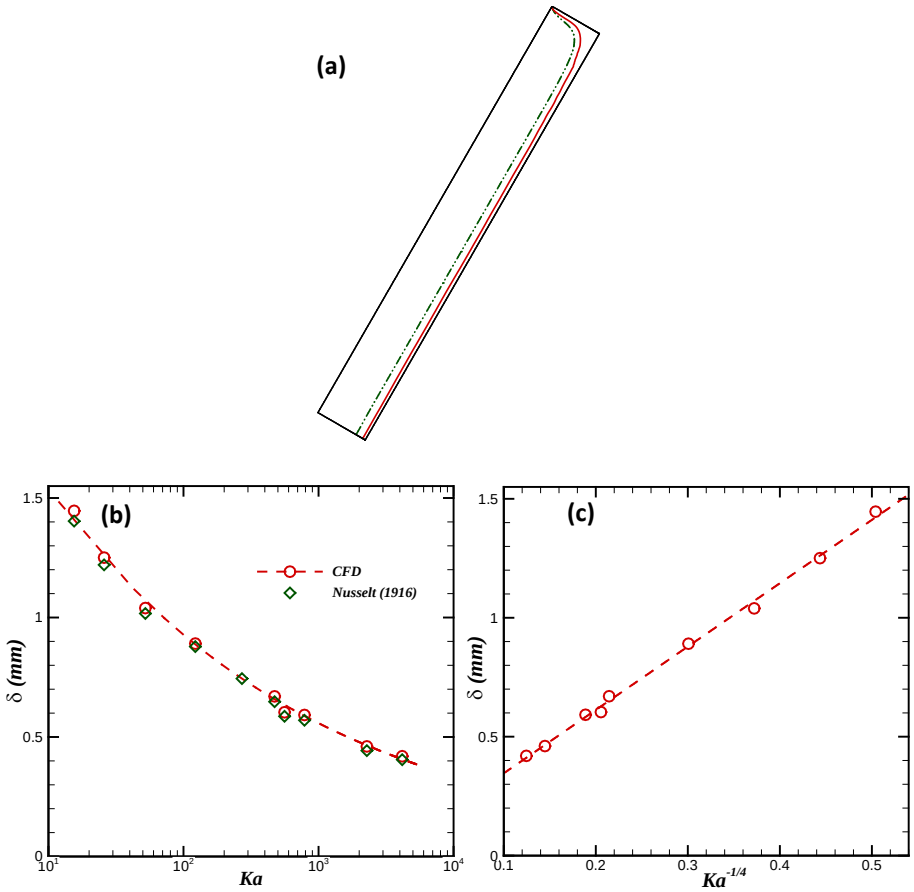

Figure 6: (a) Development of film profile over an incline plate at a fixed flow rate, red solid line: Ka=4164 and green double dotted line: Ka=15. The lower value of the Kapitza number corresponds to highly viscous solvent. (b) Comparison of the computed film thickness with Nusselt theory [26] at different Kapitza numbers. (c) Scaling of the film thickness with Ka shows the relation as $\delta \sim 1/\mathrm{Ka}^{1/4}$.

In the above analysis the impact of solvent properties on film thickness was examined for a fixed flow rate. This analysis was repeated for two other fixed We numbers (Figure 7). The same scaling behavior is revealed. Further analysis reveals the following relation for film thickness with flow rate and Kapitza number:

$$\delta \sim \frac{Q^{1/3}}{Ka^{1/4}}.$$

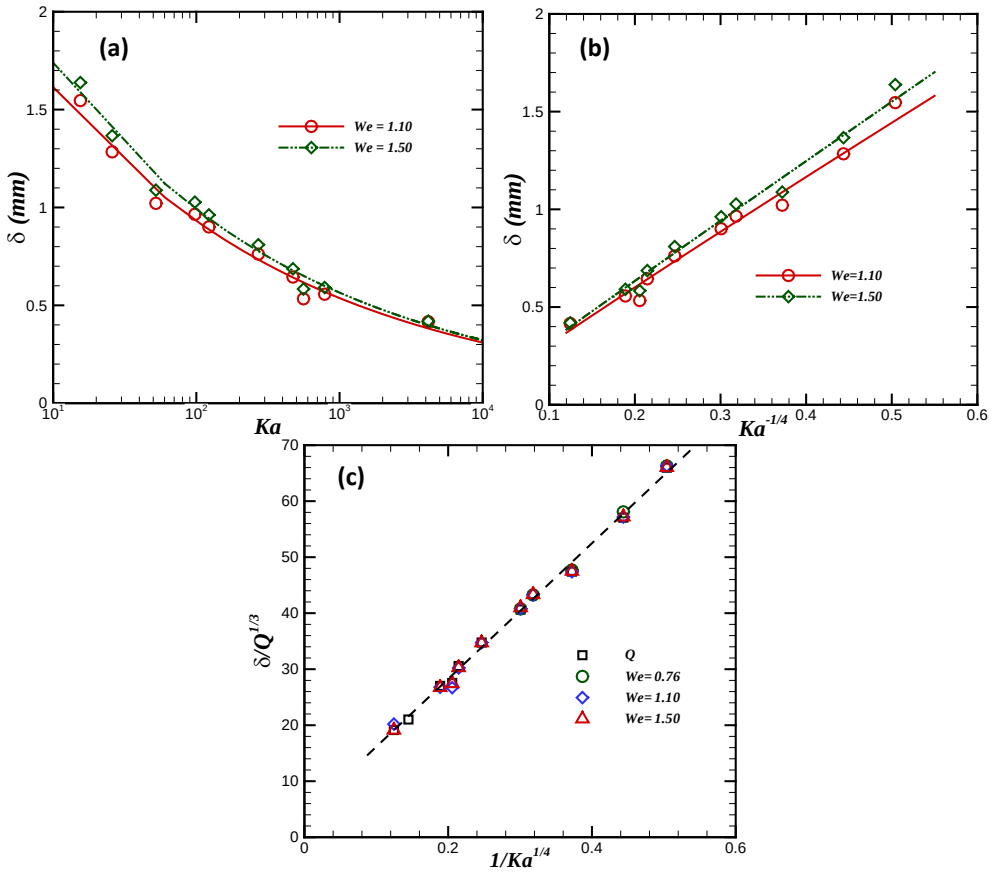

Figure 7: (a) Variation of the computed film thickness with Kapitza number at two Weber number. Note that at both We values, the plate is fully wetted. (b) Scaling of the film thickness with Ka shows relation as $\delta \sim 1/\mathrm{Ka}^{1/4}$. (c) Scaling of film thickness and flow rate with Ka.

In the above analysis of full film flow, the plate inclination angle (θ) was held constant at 60°. However, the effect of plate inclination angle on the film flow thickness was also briefly investigated. This parameter is an important aspect that dictates the flow distribution in a structured packing column and subsequently the efficiency of the column. Typically the corrugated sheets are arranged in different orientations within the packing. In view of this the inclination angle of the plate was varied from 30° to 75°. By changing the inclination angle the effects of gravity are altered. Nusselt film theory predicts that the film thickness will decrease with increased inclination angle, which is attributed to an enhanced film velocity. A significant impact on the film thickness is observed in the initial increment with film thickness decreasing with increasing inclination up to $\theta \leq 60^{\circ}$ (figure not shown).

6.2.2 Interfacial and Wetted Area

Previously, film thickness for a fully wetted plate (using relatively high Weber number) was examined using an inlet spanning the width of the domain. This setup does not show the variation in the interfacial or wetted area with solvent properties. To examine this aspect a smaller inlet was employed (see Figure 8(a)) resulting in a rivulet flow down the plate. The dimensions of the reduced inlet area are 2 mm in height and 4 mm

in width. With this setup the variation of normalized interfacial (A_{In}) and wetted area with Ka at a fixed flow rate may be analyzed. The interfacial and wetted area of the rivulet is normalized by the area of the plate. These simulations are conducted for a sufficiently long time (t_s) so that a steady value of the wetted area and exit flow rate is achieved. The value of t_s decreases with increasing value of Ka (decreasing viscosity), that is, highly viscous solvents require a longer time to reach steady state (Figure 8(b)). This behavior is consistent with what was observed in the case of the fully wetted plate discussed above.

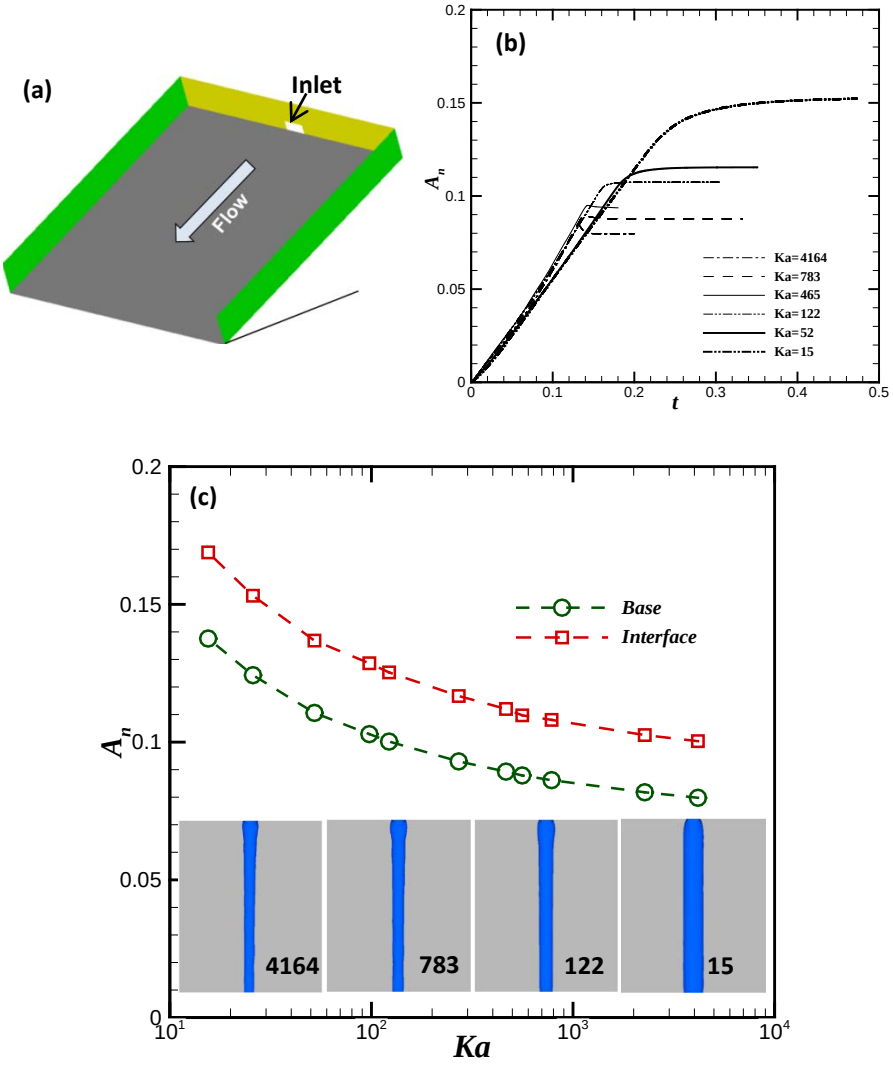

Figure 8: (a) Schematic of the flow domain used for the study of rivulet flow. (b) Transient evaluation of the wetted area of the plate for different solvents. (c) Variation of the interfacial and wetted area of plate with Kapitza number at fixed flow rate 2×10^{-6} m^3/sec. Inset shows shape of interface (f = 0.50) for different solvents.

As shown in Figure 8(c) the simulations predict a decrease in interfacial and wetted areas with increased Ka. As expected, value of the interfacial area is always greater than the wetted area. The inset of Figure 8(c) clearly shows that rivulets become wider with increased Ka. Recall that increased Ka value corresponds to reduced solvent viscosity. Given the active role of interfacial area on transport phenomenon such as heat and mass

transfer and chemical reaction, only variation in the interfacial area is discussed hence forth. Variation in regard to wetted area follows a similar pattern as interfacial area.

The effect of inlet size on the resulting rivulet flow was also examined at a fixed flow rate to ensure the above noted behavior is universal. In this analysis the height of the inlet is kept constant at 2mm and the width is varied. To achieve a fixed flow rate for varying inlet size the inlet velocity was adjusted accordingly. Figure 9(a) demonstrates that the interfacial area decreases with increased value of Ka for all inlet sizes examined. For all Ka number only a slight increase in the interfacial area is observed with increased inlet size and this is due to entrance effects. As shown in Figure 9(c), for Ka=15, the wider inlet requires more longitudinal distance to become a developed rivulet but the developed width of the rivulet remains the same for a fixed flow rate regardless of the inlet size. In this figure the developed width of the rivulet corresponding to inlet width of 4mm is compared to that with other inlet widths. As evident, the final rivulet width is the same for all cases. The height of the developed rivulet also remains the same for all cases. This is a very useful observation for solvent distribution in a structured packed column. Finally scaling for the interfacial area (Figure 9(b)) with Kapitza number shows that $A_{In}\sim 1/\mathrm{Ka}^{1/2}$. In the analysis to follow the area of the inlet is kept fixed at 2 x 20 mm.

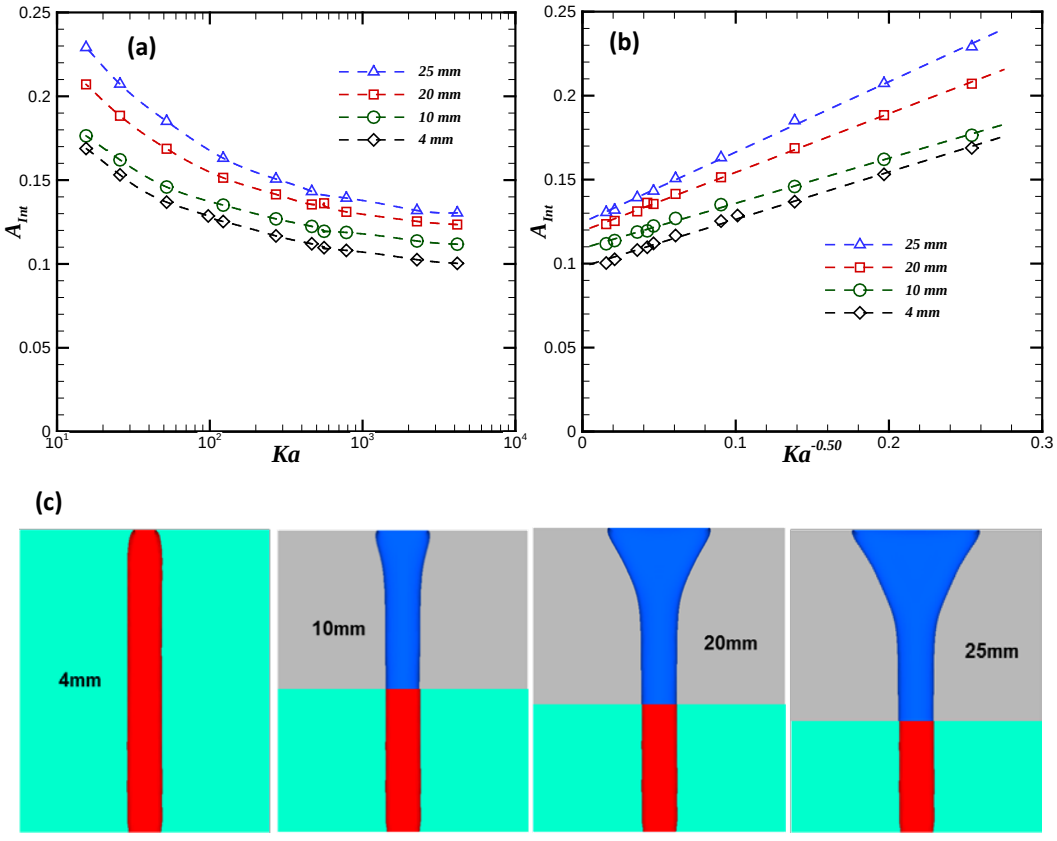

Figure 9: (a) Variation of the normalized interfacial area with Kapitza number for different inlet widths at fixed flow rate 2×10^{-6} m^3/sec. (b) Scaling for the variation of the interface area with Ka shows that $A_{In}\sim 1/\mathrm{Ka}^{1/2}$. (c) Shape of the interface (f=0.50) for different inlet width at Ka=15. The developed width of the rivulet is insensitive to inlet size at a fixed flow rate.

In the proceeding section the impact of solvent properties on normalized interfacial area was examined for a fixed flow rate. This analysis was repeated here but for two other fixed flow rates with fixed inlet size (2x20mm). The same scaling behavior as before is revealed (Figure 10). Further analysis shows that the normalized interfacial area varies with flow rate and Kapitza number as $A_{In} \sim Q^{1/3}/\mathrm{Ka}^{1/2}$.

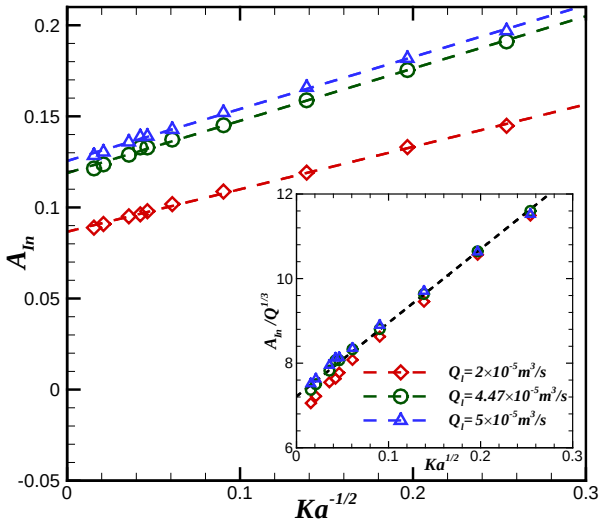

Figure 10: Variation of the normalized interfacial area with Kapitza number for different flow rate at inclination angle 60° and fixed inlet size (2x20mm).

As in the case of full film flow, the effect of plate inclination angle (θ) on the hydrodynamics of rivulet flow was also investigated. Figure 11 plots the variation of normalized interfacial area as a function of Ka for different θ varying from 30° to 75°. As can be expected, the interfacial area deceases with increased θ. Note that the change in inclination angle alters the gravitational force with an increased value of θ corresponding to a higher value of film velocity. The decrease in interfacial area is more pronounced at low Ka value. In the inset of Figure 10, the percentage change in interfacial area, $\Delta A_{In} = \dfrac{(A_{In} - A_{In60})}{A_{In60}} \times 100$, is presented, where A_{In60} is the interfacial area corresponding to $\theta = 60°$. As evident the change in interfacial area is not significant beyond an inclination angle of 60°.

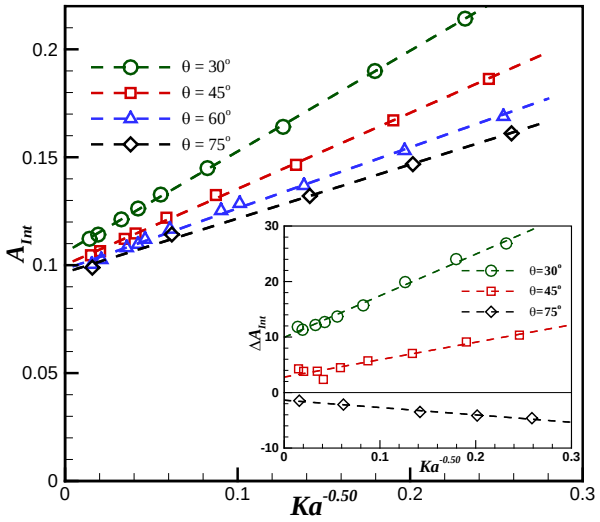

Figure 11: Variation of A_{In} with Ka for different inclination angles at a flow rate 2×10^{-6} m^3/sec and fixed inlet size (2x20mm). Inset show the percentage change in the interfacial area with respect to the interfacial area corresponding to θ=60°.

6.3 Effect of Contact Angle

As mentioned earlier the adhesive forces acting on the gas and liquid at the wall is described using a specified contact angle. The interface where solid, liquid and vapor coexist is the contact line. The contact angle defines the angle formed by the intersection of the liquid-solid interface and the liquid vapor interface. The contact angle indicates the degree of wetting when a solid and liquid interact. Large contact angles (>90) corresponds to lower wettability. Small contact angles (<90) correspond to higher wettability. The contact angle of a liquid drop on an ideal surface can be defined by a mechanical equilibrium of the drop under the action of three interfacial tensions: $\sigma_{lv}\cos y = \sigma_{sv}-\sigma_{sl}$, where σ_{lv}, σ_{sv} and σ_{sl} are the surface tension forces between the liquid-vapor, the solid-vapor and the solid-liquid, respectively. Young's equation [30] reveals a relationship between contact angle and three interfacial tensions. In practice, however the observed contact angles are not equal to that defined by Young's equation. In addition, contact angle hysteresis occurs that is generally considered to arise from either surface roughness or heterogeneity of the surface [29, 31]. Recent work indicates that the surface tension is expected to be a characteristic of a given solid-liquid system in a specific environment [32]. For a given solid, the measured contact angles do not vary randomly upon the testing liquid [25]. The value of $\cos(\gamma)$ and σ was observed to follow a linear tend for a homogenous series of liquids. In this view, lower values of σ correspond to smaller contact angles γ [25].

Thus far the simulation results have been restricted to 70° contact angle because little data for the contact angle of aqueous solvents exists in the open literature. However, the contact angle is an important property of the solvent that dictate the wetting of surface. In this context, an extensive series of simulations was conducted to investigate the effect of contact angle on wetting phenomenon. From these results an empirical theory capable of calculating the wetted and interfacial areas for any solvent and contact angle is proposed.

The effects of contact angle on the hydrodynamics in the fully wetted plate case are studied first. The simulations were conducted for two contact angles 70° and 40° at a fixed flow rate of 1.05×10^{-5} m^3/s. The value of δ as a function of Ka remains unchanged for both contact angles (see Figure 13) indicating that the contact angle does not impact the resulting the film thickness. However, the time needed for the system to achieve a fully wetted plate increases with decreasing contact angle (Figure not shown).

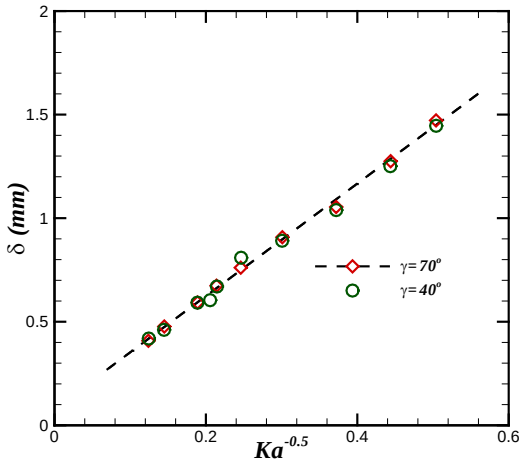

Figure 12: Variation of the computed film thickness with Kapitza numbers at two contact angles for the fully wetted plate at fixed flow rate of 1.05×10^{-5} m^3/s.

Next the effects of contact angle on the hydrodynamics of a partially wetted plate are examined. In this case simulations are conducted over a wide range of contact angles ($30 - 80^{o}$) at a fixed flow rate ($2.0 \times 10^{-6} m^3/s$) and inlet area (2x20mm) for each solvent. In Figure 13(a) the wetted and interfacial areas are plotted against the contact angle for a single solvent having Ka=15. This Ka corresponds to a solvent with low surface tension and high viscosity. The simulations show that both areas decrease with increasing contact angle, which is as expected since surface wettability should decrease with increasing contact angle. The simulations do reveal that the variation of the wetted area with contact angle is steeper than that for the interfacial area. Consequently, the difference between the wetted and interfacial areas increases with increasing contact angle. This behavior leads to an increase in film thickness, which can be understood from considering the curvature of the interface increases with increased contact angle.

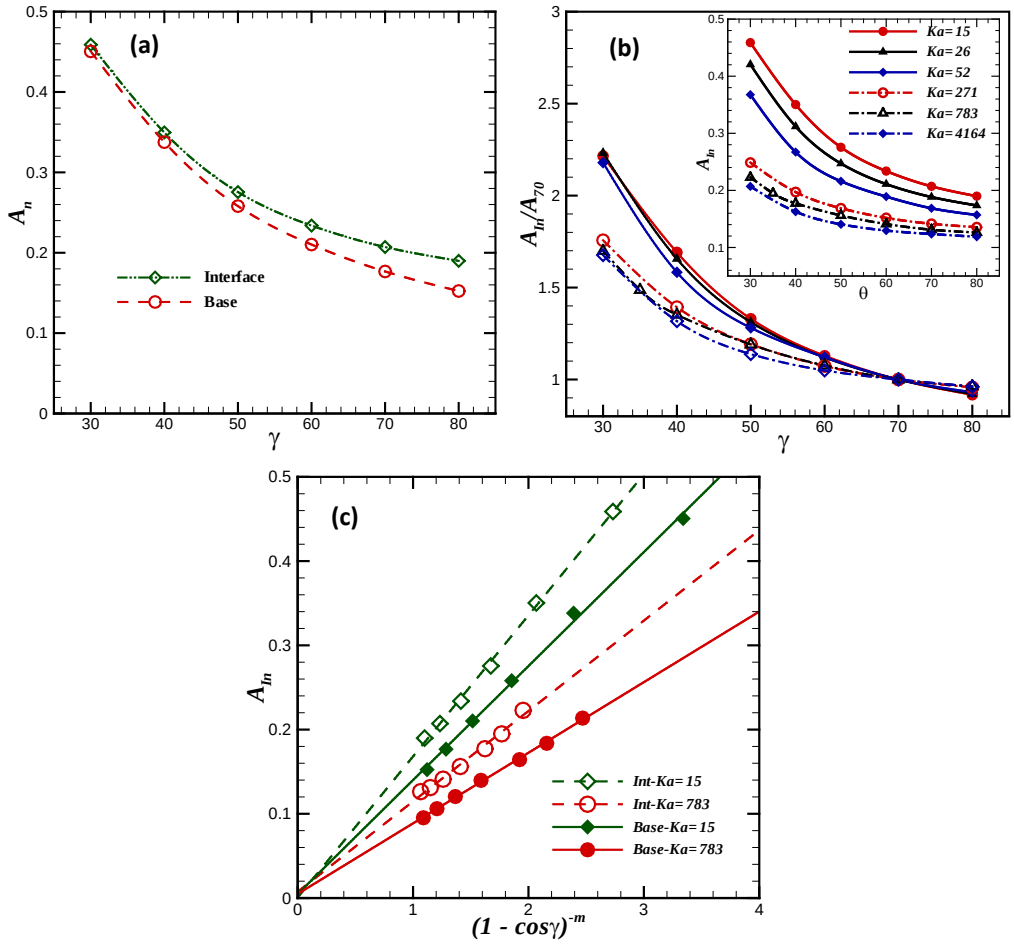

Figure 13: (a) Variation of the Interfacial and wetted areas with contact angle. (b) Variation in interfacial area normalized with respect to the interfacial area corresponding to $\gamma = 70^o$. (c) Scaling of the interfacial and wetted areas with $(1–\cos\gamma)^{-m}$ for 2 solvents having Ka=15 (low σ) and Ka=783 (high σ).

In the inset of Figure 13(b) the variation of the interfacial area with contact angle for six solvents is presented. All show a decrease in area with increased contact angle, however, some separation of the curves depending on the value of the Kapitza number is revealed. This aspect is further analyzed by renormalizing the interfacial area with the interfacial area (A_{70}) corresponding to $\gamma = 70^o$. As a result the top three and bottom three curves merge and two regimes of solvent clearly exist depending on the surface tension. Those with low surface tension (~35Nm/m; lower Ka) show steeper variation of interfacial area and wetted area with contact angle, while solvents having medium (50mN/m; higher Ka) and higher surface tension respond more slowly with contact angle. Also apparent solvents with low surface tension exhibit higher interfacial area compared to those with high surface tension.

Following the work of Zismann [33], who present a relationship between the contact angle and surface wettability, the interfacial and wetted areas were scaled as a function of $(1–\cos\gamma)^{-m}$. So that

$$A \sim 1/(1 - cos\gamma)^m \quad (8)$$

Analysis of the current results show that for wetted area (A_n)

$$\begin{aligned} m &= 0.60 \quad \sigma \leq 50\text{mN/m (low)} \\ &= 0.45 \quad \sigma > 50\text{mN/m (high)} \end{aligned} \tag{9}$$

and for interfacial area (A_{In})

$$\begin{aligned} m &= 0.50 \quad \sigma \leq 50\text{mN/m (low)} \\ &= 0.33 \quad \sigma > 50\text{mN/m (high)} \end{aligned} \tag{10}$$

These correlations are shown in the Figure 14(c) for two solvents with Ka=15 and Ka=783. These relations are observed to hold strongly. Ultimately, the correlation reflects higher interfacial and wetted areas for solvents with smaller σ and steeper variation for wetted area than interfacial area. Nicolaiewsky et al [9] and Shi and Mersmann [29] also examined the impact of the contact angle but on the film width as opposed to interfacial area. In both of their studies a single value of the exponent (*m)* was shown for a wide range of the properties. In contrast, the present study clearly establishes two values of the exponent *m* depending on the surface tension (medium/high or low).

Earlier, the normalized interfacial and wetted area were shown to vary as $A_{In} \sim 1/\mathrm{Ka}^{1/2}$ for a fixed contact angle of 70^{o} (see, for example, Figure 9(b) or 10). This relation was found to hold for all contact angles tested as demonstrated in the inset of Figure 14(a) and 14(b). Combining the expression for wetted and interfacial area as function of Kapitza number with those as function of contact angle all curves collapse into single one. Figure 14(a) and (b) show the variation of $A(1-cos\gamma)^m$ as a function of $\mathrm{Ka}^{-1/2}$ for wetted and interfacial areas, respectively. Thus, a single line of variation for either wetted or interfacial area is obtained for all contact angle and solvents as $A \sim (1-cos\gamma)^{-m}\mathrm{Ka}^{-1/2}$. The final relation for wetted and interfacial area is as follows with m defined in equations 7 and 8:

$$A_{In} \sim \frac{Q^{1/3}}{Ka^{1/2}(1-\cos\gamma)^m} \tag{11}$$

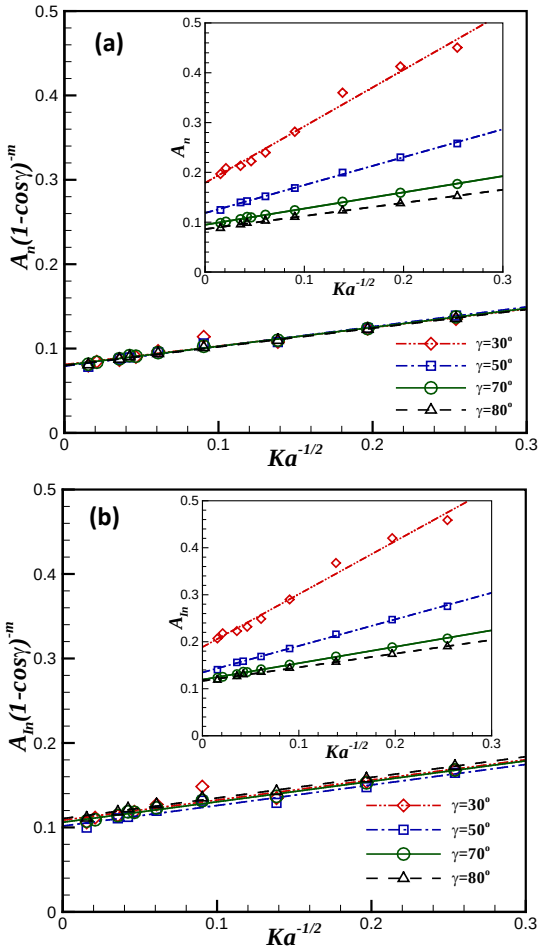

Figure 14: Scaling (a) wetted area and (b) interfacial area with contact angle and Kapitza number. For an inclined plate having θ = 60° at a fixed flow rate and inlet area (2x20mm).

7. Final Summary

The behavior of the liquid film on structured packing is a key aspect to the overall efficiency of the column for CO_2 absorption. In this effort the effects of solvent properties and contact angle (γ) on the hydrodynamics of film flow are systematically investigated using Volume of Fluid (VOF) multiphase flow simulations of film flow down an inclined plate. The simulation results were compared with available experimental results for validation of the methodology. The predicted wetted area of the plate matches well with the experimental results of the Hoffman et al [27].

A scaling analysis for film thickness and interfacial area was performed on the simulation results. Accordingly, a theory for film thickness and wetted area in terms of Kapitza number (Ka) is proposed. The advantage of the Kapitza number is that it only depends on fluid properties and independent of flow parameters. Therefore the Ka becomes fixed for a given solvent and it decreases with increasing solvent viscosity. The results show that for a fully wetted plate the film thickness (δ) decreases with increasing Ka number as $\delta \sim 1/Ka^{1/4}$. For

rivulet flow (or partially wetted plate) the interfacial area is found to decrease with increasing Ka number and scaling shows the relation $A_{int} \sim 1/Ka^{1/2}$.

These analyses are based on simulations at fixed contact angle; however, the effect of varying contact angle on the hydrodynamics was also investigated. The contact angle has negligible impact on the film thickness for the case of a fully wetted plate but strongly influences the interfacial area for the case of partially wetted plate. For rivulet flow the interfacial area increases with increasing contact angle and scaling analysis shows the relation $A_{Int} \sim 1/(1-\cos\gamma)^{m}$. The value of exponent m depends on the Ka number and shows two values, one for medium to high surface tension and another for low surface tension values.

References

1. Raynal, L., F. Ben Rayana, and A. Royon-Lebeaud, *Use of CFD for CO(2) absorbers optimum design : from local scale to large industrial scale.* Greenhouse Gas Control Technologies 9, 2009. **1**(1): p. 917-924.
2. Raynal, L. and A. Royon-Lebeaud, *A multi-scale approach for CFD calculations of gas–liquid flow within large size column equipped with structured packing.* Chemical Engineering Science, 2007. **62**(24): p. 7196-7204.
3. Ataki, A. and H.J. Bart, *The use of the VOF-model to study the wetting of solid surfaces.* Chemical Engineering & Technology, 2004. **27**(10): p. 1109-1114.
4. Gu, F., et al., *CFD Simulation of Liquid Film Flow on Inclined Plates.* Chemical Engineering & Technology, 2004. **27**(10): p. 1099-1104.
5. Iso, Y. and X. Chen, *Flow Transition Behavior of the Wetting Flow Between the Film Flow and Rivulet Flow on an Inclined Wall.* Journal of Fluids Engineering-Transactions of the Asme, 2011. **133**(9).
6. Roy, R.P. and S. Jain, *A study of thin water film flow down an inclined plate without and with countercurrent air flow.* Experiments in Fluids, 1989. **7**(5): p. 318-328.
7. Valluri, P., et al., *Thin film flow over structured packings at moderate Reynolds numbers.* Chemical Engineering Science, 2005. **60**(7): p. 1965-1975.
8. Lan, H., et al., *Developing Laminar Gravity-Driven Thin Liquid Film Flow Down an Inclined Plane.* Journal of Fluids Engineering-Transactions of the Asme, 2010. **132**(8).
9. Nicolaiewsky, E.M.A., et al., *Liquid film flow and area generation in structured packed columns.* Powder Technology, 1999. **104**(1): p. 84-94.
10. Xu, Y.Y., et al., *Portraying the Countercurrent Flow on Packings by Three-Dimensional Computational Fluid Dynamics Simulations.* Chemical Engineering & Technology, 2008. **31**(10): p. 1445-1452.
11. Iso, Y., et al., *Numerical and Experimental Study on Liquid Film Flows on Packing Elements in Absorbers for Post-combustion CO2 Capture.* Energy Procedia, 2013. **37**(0): p. 860-868.
12. Sebastia-Saez, D., et al., *3D modeling of hydrodynamics and physical mass transfer characteristics of liquid film flows in structured packing elements.* International Journal of Greenhouse Gas Control, 2013. **19**(0): p. 492-502.
13. Podowski, M.Z. and A. Kumbaro, *The Modeling of Thin Liquid Films Along Inclined Surfaces.* Journal of Fluids Engineering, 2004. **126**(4): p. 565-572.
14. Zhou, D.W., T. Gambaryan-Roisman, and P. Stephan, *Measurement of water falling film thickness to flat plate using confocal chromatic sensoring technique.* Experimental Thermal and Fluid Science, 2009. **33**(2): p. 273-283.
15. Cooke, J.J., et al., *Gas-liquid flow on smooth and textured inclined planes.* World Academy of Science, Engineering and Technology, 2012. **6**(8): p. 1449-1457.
16. Hirt, C.W. and B.D. Nichols, *Volume of fluid (VOF) method for the dynamics of free boundaries.* Journal of Computational Physics, 1981. **39**(1): p. 201-225.
17. *ANSYS FLUENT Theory Guide*. 2011.
18. Brackbill, J.U., D.B. Kothe, and C. Zemach, *A continuum method for modeling surface tension.* Journal of Computational Physics, 1992. **100**(2): p. 335-354.
19. Maham, Y., et al., *Volumetric properties of aqueous solutions of monoethanolamine, mono- and dimethylethanolamines at temperatures from 5 to 80 °C I.* Thermochimica Acta, 2002. **386**(2): p. 111-118.

20. Tahery, R. and H. Modarress, *A new and a simple model for surface tension prediction of water and organic liquid mixtures.* Iranian Journal of Science and Technology Transaction B-Engineering, 2005. **29**(B5): p. 501-509.
21. Yu, C.H., H.H. Cheng, and C.S. Tan, *CO2 capture by alkanolamine solutions containing diethylenetriamine and piperazine in a rotating packed bed.* International Journal of Greenhouse Gas Control, 2012. **9**: p. 136-147.
22. Murshid, G., et al., *Thermo physical analysis of 2-amino-2-methyl-1-propanol solvent for carbon dioxide removal.* Chemical Engineering Transactions, 2011. **25**: p. 45-50.
23. Muhammad, A., et al., *Viscosity, Refractive Index, Surface Tension, and Thermal Decomposition of Aqueous N-Methyldiethanolamine Solutions from (298.15 to 338.15) K.* Journal of Chemical & Engineering Data, 2008. **53**(9): p. 2226-2229.
24. Rayer, A.V., et al., *Physicochemical properties of {1-methyl piperazine (1) + water (2)} system at T = (298.15 to 343.15) K and atmospheric pressure.* The Journal of Chemical Thermodynamics, 2011. **43**(12): p. 1897-1905.
25. W. A, Z., *Relation of the Equilibrium Contact Angle to Liquid and Solid Constitution*, in *Contact Angle, Wettability, and Adhesion*. 1964, AMERICAN CHEMICAL SOCIETY. p. 1-51.
26. Nusselt, W., *Die Oberflächenkondesation des Wasserdampfes.* Zeitschrift des Vereines Deutscher Ingenieure 1916. **60**(27): p. 541–546.
27. Hoffmann, A., et al., *Fluid dynamics in multiphase distillation processes in packed towers.* Computers & Chemical Engineering, 2005. **29**(6): p. 1433-1437.
28. Hoffmann, A., et al., *Detailed investigation of multiphase (gas-liquid and gas-liquid-liquid) flow behaviour on inclined plates.* Chemical Engineering Research & Design, 2006. **84**(A2): p. 147-154.
29. Schwartz, L.W. and S. Garoff, *Contact angle hysteresis and the shape of the three-phase line.* Journal of Colloid and Interface Science, 1985. **106**(2): p. 422-437.
30. Young, T., *An Essay on the Cohesion of Fluids.* Philosophical Transactions of the Royal Society of London, 1805. **95**: p. 65-87.
31. Johnson, R.E. and R.H. Dettre, *Contact Angle Hysteresis. III. Study of an Idealized Heterogeneous Surface.* The Journal of Physical Chemistry, 1964. **68**(7): p. 1744-1750.
32. Snoeijer, J.H. and B. Andreotti, *A microscopic view on contact angle selection.* Physics of Fluids (1994-present), 2008. **20**(5): p. -.
33. *Contact Angle, Wettability, and Adhesion, Copyright, Advances in Chemistry Series*, in *Contact Angle, Wettability, and Adhesion*, F. Gould Robert, Editor. 1964, AMERICAN CHEMICAL SOCIETY. p. i-iii.